Geoderma 376 (2020) 114495

Contents lists available at ScienceDirect

Geoderma

journal homepage: www.elsevier.com/locate/geoderma

Predictive modeling of bedrock outcrops and associated shallow soil in upland glaciated landscapes

Olivia L. Fraser[a,b,*], Scott W. Bailey[c], Mark J. Ducey[a], Kevin J. McGuire[d]

[a] Department of Natural Resources and the Environment, University of New Hampshire, 56 College Road, Durham, NH 03824, United States
[b] White Mountain National Forest, USDA Forest Service, 71 Mountain Drive, Campton, NH 03223, United States
[c] Northern Research Station, USDA Forest Service, 234 Mirror Lake Road, North Woodstock, NH 03264, United States
[d] Department of Forest Resources and Environmental Conservation and Virginia Water Resources Research Center, Virginia Tech, Blacksburg, VA 24061, United States

ARTICLE INFO

Handling Editor: Cristine Morgan

Keywords:
Bedrock outcrops
Shallow soils
Predictive modeling
Lidar
Topographic metrics
Digital soil mapping

ABSTRACT

Identifying the areal extent of bedrock outcrops and shallow soils has important implications for understanding spatial patterns in vegetation composition and productivity, stream chemistry gradients, and hydrologic and soil properties of landscapes. Manual methods of delineating bedrock outcrops and associated shallow soils are still commonly employed, but they are expensive to implement over broad areas and often limited by representation of polygon units. Few studies have automated the delineation of bedrock outcrops. These focused on delineation approaches in landscapes with rapidly eroding hillslopes and sparse vegetation. The objectives of this study were to assess the accuracy of visually interpreting high-resolution relief maps for locating bedrock outcrops and associated shallow soil (BOSS) < 50 cm deep in a heavily forested landscape, to use visually interpreted point locations to train predictive models, and to compare predictions with manually delineated polygons in upland glaciated landscapes. Visual interpretation of Lidar-derived 1 m shaded relief maps at Hubbard Brook Experimental Forest (HBEF), USA resulted in a 79% accuracy of interpreting deep soil locations and 84% accuracy in distinguishing BOSS. We explored four probabilistic classifications of BOSS using multiple Lidar-derived topographic metrics as predictive variables. All four methods identified similar predictors for BOSS, including slope and topographic position indices with a 15, 100 and 200 m circular analysis window, respectively. Although all classifiers yielded similar results with little difference in interpretation, a generalized additive model had slightly higher accuracy predicting BOSS presence, yielding 85% overall accuracy using independent validation data across the primary study area, and 86% overall accuracy in a second validation area.

1. Introduction

Bedrock outcrops emerge at Earth's surface where weathering processes have greater potential to alter exposed bedrock than bedrock covered with regolith (Humphreys and Wilkinson, 2007). In recently glaciated landscapes, processes of glacial and post-glacial erosion and deposition are likely as important as weathering in determining the location and extent of bedrock outcrops and associated shallow soils (BOSS). Differences in weathering processes as well as moisture and physical characteristics of shallow soils have important implications for understanding spatial patterns in vegetation composition and productivity (Hahm et al., 2014; Kruckeberg, 2002; Meyer et al., 2007; Sheffer et al., 2013), influencing water quality, runoff, and storage (Asano et al., 2009; McNamara et al., 2011), and controlling soil development (Sommer et al., 2000) and regolith thickness (Karlsson et al., 2014; Shangguan et al., 2017). Therefore, identifying the areal extent of BOSS is important to ecology, hydrology, and pedology.

In the northeastern USA as in other glaciated regions, vegetation often reflects the physical and chemical conditions determined by dominant geomorphic processes. In this region, forest types near bedrock outcrops are commonly found to have successional stands of coniferous trees, with a prevalence of spruce-fir-birch-red maple in shallow soils (Smith, 1995). Mixtures of deciduous trees, especially sugar maple and oaks are found in deeper soils (Leak, 1982). In addition, areas dominated by bedrock outcrops limit deep percolation, forcing lateral hydrological movement of groundwater through the rooting zone (Gannon et al., 2014) and controlling spatial patterns in carbon and metal sequestration in soil profiles (Bailey et al., 2014; Bourgault et al., 2017; Sommer et al., 2001). Distance from bedrock controlled-areas and proportion of bedrock outcrops in upslope drainage areas have been used to explain vertical and horizontal soil variability at the catchment scale (Gillin et al., 2015). Finally, primary

* Corresponding author.
E-mail address: olivia.fraser@usda.gov (O.L. Fraser).

https://doi.org/10.1016/j.geoderma.2020.114495
Received 13 October 2019; Received in revised form 19 May 2020; Accepted 28 May 2020
Available online 17 June 2020
0016-7061/ Published by Elsevier B.V.

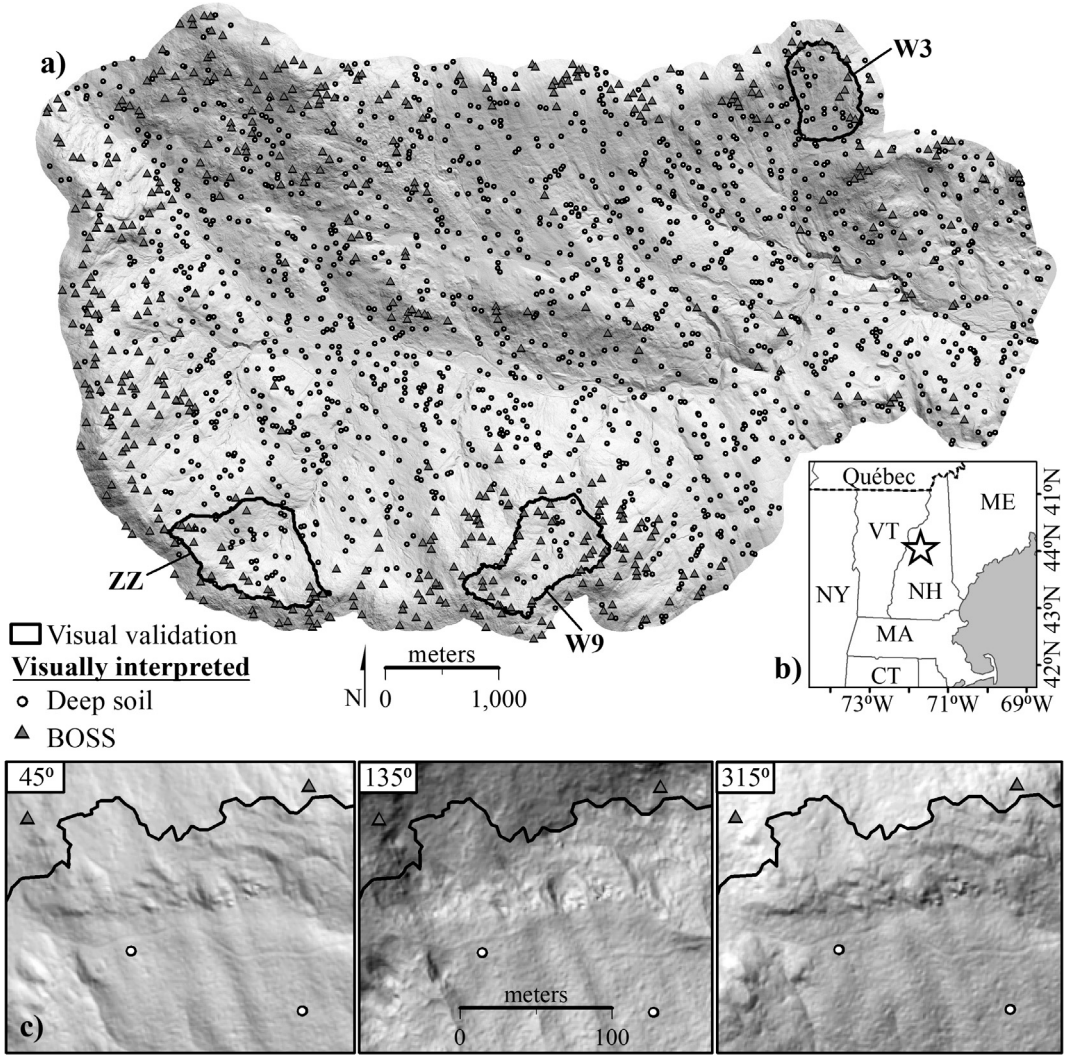

Fig. 1. (a) Hillshade (315° illumination angle) of Hubbard Brook Experimental Forest (HBEF) buffered by 200 m and the 2000 randomly generated points used for visual interpretation of bedrock outcrops and associated shallow soil (BOSS) locations. The solid black outlines indicate the three subcatchments selected for validation of shaded relief visual interpretations. (b) Vicinity inset depicts the location of HBEF (43°56′N, 71°45′W) marked by a five-point star within the northeastern USA. (c) Three figure insets display hillshades (illumination angles 45°, 135°, and 315°) of northern W3 at a 1:5000 absolute scale.

mineral dissolution and soil development near bedrock outcrops can explain the longitudinal variation of headwater stream chemistry, setting regional background water quality characteristics (Bailey et al., 2019).

Bare earth models derived from Light detection and ranging (Lidar) provide a unique opportunity for bedrock and surficial geologic mapping where underlying geomorphic patterns are visible despite dense vegetation cover (Webster et al., 2006). A high-resolution digital elevation model (DEM) can be derived from the Lidar ground returns and represents Earth's bare surface. Computational algorithms are often used to automate the extraction of various terrain features from Lidar DEMs (Drăguţ and Eisank, 2011; MacMillan et al., 2000). The resulting terrain features have been classified to predict a wide range of soil properties including hydrologic influences on soil formation using multinomial logistic regression in New Hampshire, USA (Gillin et al., 2015), historical extent of Spodosols using random forests in West Virginia, USA (Nauman et al., 2015), digital soil mapping using support vector machines in British Columbia, Canada (Heung et al., 2016), soil depth with generalized additive models in Idaho, USA (Tesfa et al., 2009) and a regolith thickness model in Sweden (Karlsson et al., 2014). The role of terrain features as covariates in digital soil mapping approaches, however, vary widely with the scale and resolution of the soil property predicted (McBratney et al., 2003). Additionally, the wide availability of Lidar DEMs has highlighted the influence of spatial resolution and scale on modelling (Behrens et al., 2010; Cavazzi et al., 2013; Minasny and McBratney, 2016).

Bedrock outcrops can be visually distinguished in Lidar-derived DEMs based on the rough topographic expression along exposed ridges of upper portions of slopes with convex curvature. Extracting bedrock outcrop features, however, is especially challenging in landscapes where outcrops are scattered and where associated thin soils constitute a thin mantle over shallow bedrock, resulting in a topographically smooth appearance in a shaded relief map rather than the common rough topographic expression of exposed outcrops. Since the areal extent of bedrock outcrops serves as a predictor of various biotic and abiotic properties, a few studies have explored automating the delineation of bedrock outcrops by leveraging the spectral characteristics of exposed rock using high-resolution panoramic photographs (DiBiase et al., 2012) and image classification techniques (Scarpone et al., 2017). Additionally, Milodowski et al. (2015) created a roughness metric based on the rough expression and slope associated with bedrock demonstrating that the local variability of surface normal vectors can be used as a topographic signature to identify rock exposure. However, the challenge to delineate bedrock outcrops remains in landscapes with

Table 1
Dataset name, reference, sample design, sample size (n), and purpose in this study.

Name	Reference	Sample design	n	Purpose
Visual interpretation	This study	Randomly generated	2000	Training/testing
Visual interpretation subset	This study	Randomly selected subset	325	Visual interpretation validation
Field verification	This study	Randomly selected subset	51	Visual interpretation field validation
Hubbard Brook Experimental Forest (HBEF) database	Bailey, 2019	Systematic grid	329	Independent model validation
Wild Ammonoosuc (WAMMO) database	Colter, 2019	Stratified random	176	Independent model validation
Natural Resources Conservation Service (NRCS) polygons	NRCS	Manual delineation	–	Comparison

dense canopy cover since more commonly used image classification approaches are not applicable because only a fraction of bedrock and outcrops interspersed with shallow soils are revealed. In addition, the multi-scale dependency of bedrock outcrops and associated shallow soil needs to be addressed.

Therefore, new approaches are needed to address the automatic delineation of BOSS in upland glaciated landscapes with dense vegetation cover. The first objective of this study was to assess the accuracy of visually interpreting a high-resolution DEM-derived hillshades with different illumination angles for locating BOSS. The second objective of this study was to automate the delineation of BOSS from visually interpreted training points using predictive analytics with Lidar terrain derivates as predictors. The third objective was to compare binary predictions to manually delineated polygons. This approach differs from previous digital soil mapping efforts by evaluating visually interpreted model training points and could significantly improve the statistical rigor of generating a robust sample size. Finally, we evaluated predictive performance of four classifiers with two independent validation datasets, the second being a distinct study area from where the earlier objectives were performed. This also differs from previous digital soil mapping efforts by leveraging a second geographically independent study area with a robust sample design for model evaluation.

2. Methods

2.1. Study sites

Hubbard Brook Experimental Forest (HBEF) is approximately 3175 ha within the White Mountain National Forest (WMNF) of New Hampshire, USA (Fig. 1b) with elevation ranging from 213 to 1008 m above sea level and comprising the catchment draining to third-order Hubbard Brook. The climate is humid continental with annual precipitation of 140 cm and a mean stream runoff of 90 cm (Bailey et al., 2003). Soils are mostly Spodosols with variable drainage conditions with an average 0.7 m thickness to the base of the B horizon (Bailey et al., 2014). Northern hardwood forest dominates HBEF including *Acer saccharum* Marsh. (sugar maple), *Betula alleghaniensis* Britt. (yellow birch) and *Fagus grandifolia* Ehrh. (American beech) as dominant species in deeper soils. Shallow-to-bedrock soils are often vegetated with conifer-dominated stands composed of *Picea rubens* Sarg. (red spruce), *Abies balsamea* (L.) Mill. (balsam fir), and *Betula cordifolia* Regel (mountain white birch). The forest was selectively harvested from 1880 to 1920, damaged by a hurricane in 1938, and is now relatively mature, reaching a plateau in biomass accumulation in the 1980s (Siccama et al., 2007).

Bedrock in HBEF consists of mica schist and granulite of the Silurian Rangeley Formation and granitic rocks of the Devonian Kinsman pluton (Burton et al., 2000). Bedrock is poorly exposed, outcropping mostly along ridges and in some stream channels, and covered by a veneer of glacial drift ranging up to 10 m or more in thickness (Bailey et al., 2019). Shallow soils near outcrops grade to deep soils which commonly occur along backslopes and lower landscape positions. Bedrock outcrops and associated shallow soils are defined by an average thickness of less than 50 cm to bedrock (Soil Science Division Staff, 2017).

The Wild Ammonoosuc catchment (WAMMO) was the second distinct study area used solely for predictive model evaluation (see Section 2.8). The WAMMO catchment, also in the WMNF 16.3 km northwest of HBEF, is 6883 ha with elevation ranging from 336 to 1,946 m. The dominant vegetation is similar to HBEF, and includes northern hardwood, spruce-fir, and mixed-species forests.

2.2. Sample design

BOSS were estimated to represent 40% of the study area using existing geologic maps (Burton et al., 2000). The HBEF catchment boundary was buffered by 200 m to ensure the full extent of ridges were considered. Two thousand points were randomly generated within HBEF catchment (Fig. 1a) as recommended for sampling accuracy assessment by Congalton and Plourde (2002) to capture 50 points per categorical variable. Table 1 outlines dataset names, sources, sample design, sample size, and purpose in this study.

2.3. Visual interpretation of 2000 randomly generated points

All 2,000 points were then visually interpreted as BOSS or deep soil from Lidar-derived hillshade images with three illumination angles (45°, 135°, 315°). The Lidar data were collected during leaf-off and snow-free conditions by Photo Science, Inc. in April 2012 for the WMNF using an Optech GEMINI Airborne Laser Terrain Mapper. The laser returns were recorded at an average altitude of 1158.24 m above ground level using a 30% overlap, scan angle of 27°, a nominal pulse density of 3 pulses/m^2 and a 9.25 cm vertical Root Mean Square Error.

Visual identification of BOSS regions from the Lidar-derived hillshades were defined as areas exhibiting a rough topographic expression where the underlying bedrock structure was notable. Each point was initially evaluated at 1:1000–3000 and then at a 1:6,000 absolute scale to consider the context of the surrounding landscape (Fig. 1c). We then validated the visual interpretations of the high-resolution hillshades using a subset of 325 points (Table 1). Two coauthors independently interpreted the 325 points from three subcatchment areas (Fig. 1a), representative of transition from bedrock-controlled ridge to deep soils, spanning a range of proportion of outcrops.

Glacial drift is thin in the three subcatchments and interspersed with exposed bedrock in the uppermost portions of the catchments, particularly along catchment divides while it is variable and up to 10 m thick in central to lower portions of the catchments (Bailey et al., 2019). Catchment W9 is distinct in having much more bedrock outcrops while the majority of the catchment is underlain by thin drift, with bedrock less than 1 m deep. One coauthor had extensive field experience in the three subcatchments and the other did not.

2.4. Field verification of visually interpreted points

A total of 51 points were randomly selected (Table 1) from the 325 subset points using a base package random number generator in R (R Development Core Team, 2018) for field verification of visual interpretations. The 51 subset points were located pedons using a Trimble GPS unit equipped with a Trimble Hurricane Antenna. Soil pits were hand dug at the point, approximately 0.75 × 0.5 m wide and up to 1.2 m deep, to sample the entire solum and the upper portion of the C

Table 2
Topographic metrics created from terrain analysis functions as predictor variables and associated method.

Metric	Reference
Maximum slope (%)	Travis et al. (1975)
Aspect	Stage (1976)
Topographic Ruggedness Index (TRI)	Riley (1999)
Vector ruggedness metric (VRM)	Sappington et al. (2007)
Plan and Profile curvature (Plan and Prof)	Zevenbergen and Thorne (1987)
Topographic Position Index (TPI; 15, 100, & 200 m)	Guisan et al. (1999)
Topographic Wetness Index (TWId)	Hjerdt et al. (2004)

horizon or bedrock, whichever came first. Genetic horizons were sampled and described by depth, thickness, Munsell color, texture, structure, moist consistence, presence of redoximorphic features, rooting density, and coarse fragment content (Schoeneberger, 2012).

2.5. Topographic metrics

Topographic metrics (Table 2) were calculated, from a coarsened 5 m DEM using mean cell aggregation, to serve as the predictor variables. Slope (%) was calculated using the maximum slope algorithm (Travis et al., 1975). A trigonometric transformation was applied to scale aspect from −1 to 1, positions on flat ground with a value of 0 and steeper south- or north-facing slopes with a value of 1 or −1, respectively, by combining aspect and slope according to Stage (1976). Topographic ruggedness index (TRI; Riley, 1999) was created with a 3x3 neighborhood window. Vector ruggedness metric (VRM) was created using a 3x3 neighborhood window size (Sappington et al., 2007). The Zevenbergen and Thorne (1987) method was used to generate planform (Plan) and profile (Prof) curvature. Topographic position indices (TPI; Guisan et al., 1999) were created with a moving circular-window centered on a target cell using a 15, 100, and 200 m radius taking the difference between the elevation of each cell and mean elevation. Topographic wetness index (TWId; Beven and Kirkby, 1979) was computed with the upslope accumulated area using multiple triangular flow direction algorithm (Seibert and McGlynn, 2007) created from a 5 m hydroenforced DEM as the numerator and a 5 m analysis window for downslope index as the denominator (Hjerdt et al., 2004).

2.6. Predictive models

Four classification methods, or classifiers, commonly used for predicting soil properties were selected for predicting the presence of BOSS. The 2000 visually interpreted points were used for training of all classification methods. First, logistic regression (LR) was used to probabilistically model BOSS presence using the topographic metrics. Logistic regression relates the probability of occurrence in a group to a set of predictor variables using the logit transformation (Kleinbaum et al., 2013). The outputs of logistic regression are expressed in probabilistic terms where values ranging from 0 to 1 indicate probability of occurrence, with higher values representing a higher probability. Second, we used a random forests (RF) classifier which is a hierarchical non-parametric approach that uses a combination of tree predictors and the results are based on a randomized subset of the sample and predictors (Breiman, 2001; Hastie et al., 2009).

We also used a support vector machine (SVM) approach with a linear kernel which deals well with binary classification (Hastie et al., 2009). SVM uses a hyperplane to separate the binary classes and predict the maximum margin between each class based on the distance between the hyperplane and the nearest points (Hastie et al., 2009). Finally, we used a generalized additive model (GAM) which is a statistical approach that generalizes multiple regression by replacing linear combinations of the explanatory variables with combinations of nonparametric smoothing or fitting functions, estimated through backfitting algorithms (Hastie and Tibshirani, 1990; Wood, 2004). GAM was chosen due to the flexibility of the nonparametric smooth technique which allows for fitting with either linear or non-linear predictors. Generalized cross validation criteria (GCV) was used for estimating the smoothing parameter.

2.7. Statistical analysis and predictive performance

Topographic metric computations and classification approaches were implemented in R (R Development Core Team, 2018). Topographic metrics (Fraser et al., 2019a) were created from a 5 m spatial resolution DEM (Fraser et al., 2019b) using RSAGA (Brenning, 2008). RSAGA is a R package providing access to geoprocessing and terrain analysis functions of SAGA-GIS (Conrad et al., 2015). The caret package (Kuhn, 2008), with numerous prediction functions well suited for digital soil mapping (Brungard et al., 2015; Malone et al., 2017), was implemented for all four classifiers. Data were partitioned using the 70% for the training set and 30% for the testing set. The LR, RF, SVM, and GAM models were calculated using the *train* function, within the caret package which performs the training, pre-processing, tuning, and performance assessment. The predictive binary performance of all four methods, using a 0.5 probability threshold, were evaluated using a standard error matrix (Congalton, 1991) with the *confusionMatrix* function in the caret package, the coefficient of agreement (κ) (Cohen, 1960), and the 95% significance level ($p < 0.05$) of a topographic metric as an independent variable. The 2000 visually interpreted points were partitioned for cross validation and the error rates for cross-validation partitions were aggregated into a mean error rate with each classifier. Recursive feature elimination was used for models without built-in feature selection using the *rfe* function. The relative variable importance measure of each topographic metric's contribution to the accuracy was calculated using the *varImp* function. The accuracy of prediction was also evaluated using independent validation data across the primary study area and a second validation area (see Section 2.8).

2.8. Independent model evaluation

Two independent validation datasets were used to evaluate the predictive performance in two different geographic areas: HBEF and the WAMMO. First, 329 pedons (Table 1) from the HBEF soil database (Bailey, 2019) were categorized for each pedon as BOSS presence or absence. A total of 32 pedons represented BOSS and 297 pedons represented deep soil. The pedon locations from the HBEF dataset were primarily sampled following a systematic grid (Schwarz et al., 2001). The HBEF soil database includes descriptions from soil pits hand dug using the same protocol for the 51 locations (see Section 2.4). To assess all model binary predictions of BOSS, both validation datasets were partitioned based on depth to bedrock. Soil profiles with a depth to bedrock less than 50 cm were coded as presence of BOSS. Fig. 2 depicts eight representative soil profiles (plots HB035, HB051, HB125, and WS_F2) from the HBEF database selected for validating presence and absence of bedrock outcrop and associated shallow soil. Mean prediction probabilities were calculated from HBEF dataset by extracting predicted probability at each point location to evaluate probability threshold for final binary classification.

In contrast to the HBEF soil database, 176 pedon locations from the WAMMO soil database (Table 1) were sampled using a stratified random approach based on the distribution of multiple Lidar-derived topographic metrics across the WAMMO catchment (Colter, 2019). This method of stratified random sampling has been shown to reduce the overall prediction error since points are uniformly allocated over the feature space proportional to the distribution of the predictor (Brus et al., 2011; Hengl et al., 2003). Natural Resources Conservation Service (NRCS) personnel described the 176 WAMMO pedons using the same methods as HBEF soil profile descriptions (see Section 2.4). All

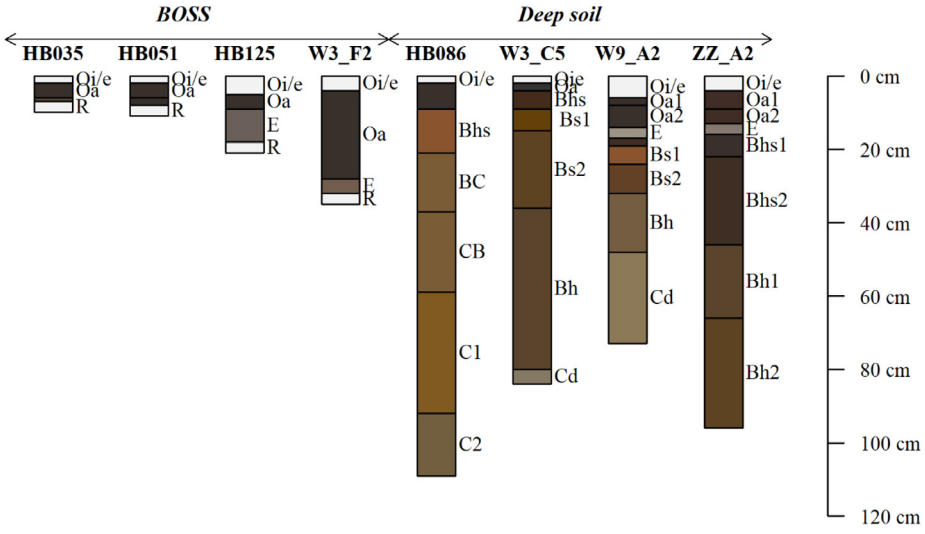

Fig. 2. Representative soil profiles (plots HB035, HB051, HB125, and W3_F2) from the HBEF database selected for validating presence of bedrock outcrop and shallow soil predictions and four soil profiles (HB086, W3_C5, W9_A2, ZZ_A2) representative of deep soils. The 'aqp' package in R was used to create Fig. 2 (Beaudette et al., 2013).

locations for pedons from HBEF and WAMMO were determined using a global positioning unit. Continuously Operating Reference Station (CORS) data from the National Geodetic Survey and differential correction software were used to obtain approximately 1–2 m horizontal precision.

2.9. Manually delineated polygons

NRCS completed a comprehensive soil parent material map (Colter, 2019), including bedrock outcrops and associated shallow soils, across portions of the WMNF. NRCS manually delineated parent material at a 1:3000–6000 absolute scale using shaded relief maps. Initial field verification was completed to assist in the manual delineation and later followed with selective field verification focusing in areas with parent material transitions.

3. Results

3.1. Evaluation of visual interpretation from shaded relief maps

A total of 525 points were visually interpreted as BOSS and 1475 points were visually interpreted as deep soil locations. The two independent observers who visually interpreted the 325 subset points had 91% agreement on BOSS. Areas with greatest disagreement typically occurred near a likely transition to deep soils or an isolated pocket of deep soil within an area surrounded by bedrock outcrops along ridges. A total of 22 of the 51 field-verified locations were deep soils and 29 were BOSS locations. Visual interpretation of shaded relief maps compared to the 51 field-verified locations yielded a 77.2% accuracy of interpreting deep soils and 82.7% accuracy in distinguishing BOSS. Field verification revealed visual interpretations of BOSS presence that were in fact deep soil inclusions (< 15 m^2; i.e. three or less pixels) surrounded by bedrock outcrops were the greatest source of error for visually identifying BOSS. There were 15 field-verified locations that were identified as deep soil inclusions predominantly surrounded by BOSS. Deep soil inclusions (< 15 m^2) surrounded by BOSS accounted for 62.5% of incorrectly interpreted BOSS locations.

3.2. Model comparison and variable importance

There were slight differences in model performance using the visually interpreted data points for training and cross validation. The LR model using slope, TPI100 (TPI with a 100 m window) and TPI200 (TPI with a 200 m window) resulted in $\kappa = 0.51$ (Table 3). Slope, TPI100, and TPI200 had relative variable importance values of 34.8, 78.1, and 100.0 respectively. LR had an overall 83.4% accuracy predicting the visually interpreted BOSS and 95.0% accuracy predicting deep soil locations. The RF model resulted in $\kappa = 0.53$, overall accuracy of 84.2% and 94.1% accuracy predicting deep soil locations. The RF model using TPI100 and TPI200 had relative variable importance values of 22.3 and 100.0 respectively. The SVM model resulted in $\kappa = 0.54$, also with the same topographic metrics as LR, overall accuracy of 84.0%, 59.0% accuracy predicting visually interpreted BOSS presence, and 92.8%, deep soil locations (Table 3). Slope, TPI100, and TPI200 had relative variable importance values of 65.8, 28.4, and 100.0 respectively. The final GAM model variables differed slightly with slope, TPI15 (TPI with a 15 m window) and TPI200, which resulted in the highest coefficient of agreement ($\kappa = 0.57$) of all four classifiers and overall accuracy 85.2% (Table 3). Slope, TPI15, and TPI200 had relative variable importance values of 68.6, 30.1, and 100.0 respectively. GAM had a 57.7% accuracy predicting the visually interpreted BOSS and 94.6% accuracy predicting deep soil locations (Fig. 3).

Table 3
Error matrix comparing bedrock outcrops and associated shallow soil (BOSS) and deep soil testing data (600 of 2000 points) to model predictions, overall model accuracy and coefficient of agreement (κ) for all four classifiers.

	Reference			
	BOSS	Deep Soil	Overall accuracy	κ
Predicted			LR	
BOSS	79	22	0.83	0.51
Deep Soil	77	422		
			RF	
BOSS	85	26	0.84	0.53
Deep Soil	71	418		
			SVM	
BOSS	92	32	0.84	0.54
Deep Soil	64	412		
			GAM	
BOSS	90	24	0.85	0.57
Deep Soil	66	420		

3.3. Independent dataset validation in two geographic areas

The HBEF validation dataset consisted of 32 pedons that represented BOSS and 297 pedons that represented deep soil locations. The LR predictions had 46.9% accuracy predicting BOSS presence compared to HBEF pedon data and 88.2% accuracy predicting deep soil locations (Table 4). RF predictions had 53.1% accuracy predicting BOSS presence compared to HBEF pedon data and 87.2% accuracy predicting

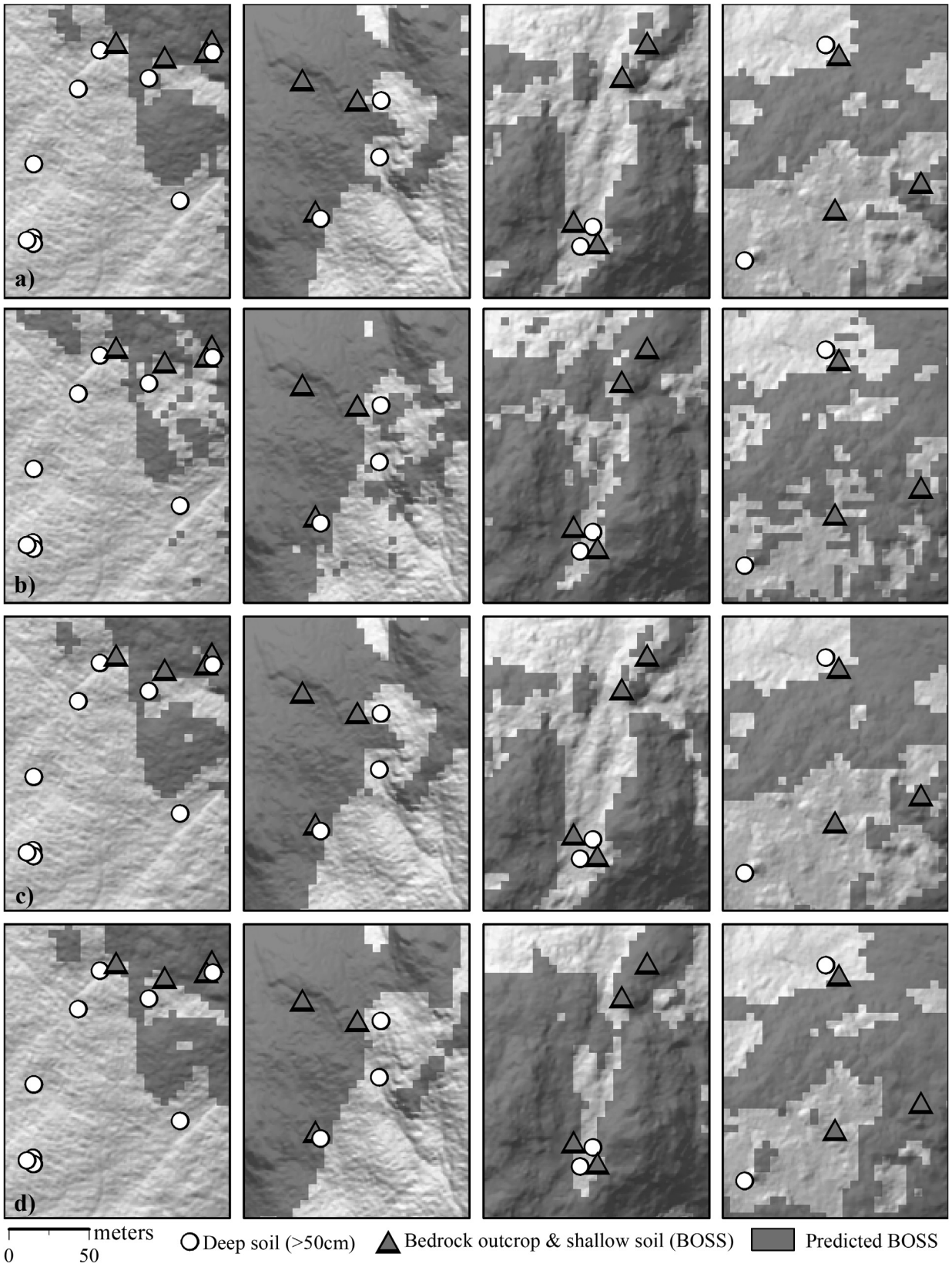

Fig. 3. Different views of a) LR, b) RF, c) SVM, and d) GAM predictions of BOSS (dark grey) across HBEF displaying independent validation data using a white circle to depict deep soil sample locations and a dark grey triangle for BOSS. The BOSS predictions (5 m spatial resolution) are depicted with a dark grey transparency over a 1 m hillshade (315° illumination angle).

Table 4
Error matrix, including overall model accuracy and coefficient of agreement (κ), for all four classifiers (Predicted) compared to independent HBEF and WAMMO soil databases (Reference).

	Reference					
	HBEF Independent validation			WAMMO Independent validation		
	BOSS	Deep Soil	Accuracy	BOSS	Deep Soil	Accuracy
Predicted				LR		
BOSS	15	35	0.84	20	10	0.85
Deep Soil	17	262		16	130	
				RF		
BOSS	17	38	0.84	17	12	0.82
Deep Soil	15	259		19	128	
				SVM		
BOSS	13	33	0.84	19	9	0.85
Deep Soil	19	264		17	131	
				GAM		
BOSS	15	31	0.85	22	11	0.86
Deep Soil	17	266		14	129	

deep soil locations. SVM had 40.6% accuracy predicting BOSS presence and 88.8% predicting deep soil locations. The GAM predictions had 46.9% accuracy predicting BOSS presence using HBEF pedon data and 89.6% accuracy predicting deep soil locations. In addition, the mean prediction probabilities for BOSS presence differed. The LR had a mean prediction probability of 0.62 for BOSS with a standard error (SE) of ± 0.03 and RF had a mean prediction probability of 0.68 (± 0.03 SE). SVM had a 0.61 mean prediction probability for BOSS presence (± 0.03 SE). Finally, GAM had a mean prediction probability of 0.72 for BOSS presence (± 0.01 SE).

The most notable differences in classifier predictions were based on expert visual comparisons when all four predictions results were compared on a 1 m hillshade (315° illumination angle). RF model predictions, and LR in some areas, resulted in heavily pixelated predictions with several isolated BOSS predicted pixels throughout the study area that were inaccurate. Numerous BOSS soil presence pixels were randomly scattered throughout deep soil predicted locations, regardless of the prediction probability. SVM and GAM predictions, however, resulted in more accurate, discrete clusters of BOSS presence. Single pixel predictions of bedrock outcrops-associated shallow presence surrounded by deep soil locations were more often predicted correctly by SVM and GAM (Fig. 3).

The WAMMO validation dataset consisted of 36 BOSS pedons and 140 pedons that represented deep soil locations. The LR predictions had 55.6% accuracy predicting BOSS presence compared to WAMMO pedon data and 92.9% accuracy predicting deep soil locations. RF had slightly lower accuracy of 47.2% predicting BOSS presence and 91.4% predicting deep soil locations in WAMMO. SVM had a 52.8% accuracy predicting BOSS presence and 93.6% accuracy predicting deep soil locations in WAMMO. Finally, the GAM predictions had 61.1% accuracy predicting deep soil locations in WAMMO and 92.1% accuracy predicting deep soil locations.

3.4. Manually delineated polygons compared to independent dataset validation

The HBEF manually delineated polygons had 71.9% accuracy identifying BOSS presence, 64.3% accuracy identifying deep soil locations, and overall accuracy 65.1% (Table 5). Fig. 4a depicts probability of BOSS from 0 to 1 with the GAM model and Fig. 4b illustrates binary GAM predictions (0.5 threshold) to manual delineation of BOSS. The overall agreement on bedrock occurrence is high, however, predicted BOSS identified higher presence of small pockets in the valley bottom and more scattered pockets of deep soil along ridges. Manually delineated polygons overestimated the presence of BOSS validation data by 28.1%.

Table 5
Error matrix, including overall accuracy, for manually delineated polygons digitized by visual interpretation of multiple 1 m Lidar-derived hillshades compared to independent HBEF and WAMMO soil database (Reference).

	Reference					
	HBEF Independent validation			WAMMO Independent validation		
Polygons	BOSS	Deep Soil	Accuracy	BOSS	Deep Soil	Accuracy
BOSS	23	106	0.65	28	19	0.85
Deep Soil	9	191		8	121	

The WAMMO manually delineated polygons had 77.8% accuracy identifying BOSS presence, 86.4% accuracy identifying deep soil locations, and overall accuracy 84.7%. Fig. 5 depicts presence of predicted BOSS from the GAM model (0.5 threshold) compared to manual delineations of BOSS in WAMMO. Manually delineated polygons overestimated the presence of BOSS validation data by 22.2%.

4. Discussion

4.1. Visual interpretation and manual delineation

Visual interpretation of terrain derivatives is commonly used for mapping of bedrock geology and soil properties (Belt and Paxton, 2005; Haugerud et al., 2003). Current bedrock geology and soil mapping efforts in the northeastern USA often requires the manual delineation of bedrock-controlled areas using visual interpretation of Lidar-derived hillshades (Shi et al., 2009) or derivatives of surficial geologic maps (McBratney et al., 2003). Since a large sample size is often required for rigorous predictive modeling, it poses a common limitation in mapping critical zone features (Hengl et al., 2003). The visual interpretation of bedrock outcrops in this study allows for a statistically valid sample size to be achieved with a high accuracy and agreement in identifying presence of BOSS. However, the greatest source of error in visually identifying BOSS from Lidar derived hillshades, at point locations in this study, occurred in deep soil inclusions (< 15 m^2) of topographically smooth areas along ridges surrounded by BOSS.

The NRCS manual delineation of BOSS polygons at HBEF (Fig. 4b) had 65.1% overall accuracy and overestimated the presence of BOSS by 28.1% in HBEF. The NRCS manual delineation of WAMMO BOSS presence (Fig. 5) was identified with 84.7% overall accuracy and manually delineated polygons overestimate the presence of BOSS by 22.2%. Although there is overall agreement on the topographic expression of BOSS visual interpretation from high-resolution hillshade maps with several illumination angles, the manual delineation of bedrock-controlled landscapes retains numerous limitations associated with the geometry, boundary, and scale of polygon units (Zhu et al., 2001). Extensive time and expertise are required for manual delineations as well as the limitations associated with polygons are related to scale influencing delineation such as small, deep soil inclusions (< 15 m^2) commonly found along ridges. This study demonstrates visually interpreting BOSS point locations from Lidar-derived hillshade maps to achieve a robust sample size for predictive analytics are comparable to manual delineation of polygons depending on the geometry and scale needed.

4.2. Comparison with other regions

Only a few studies have explored automating the delineation of bedrock outcrops. For example, Milodowski et al. (2015) created a computational algorithm for calculating a roughness metric which

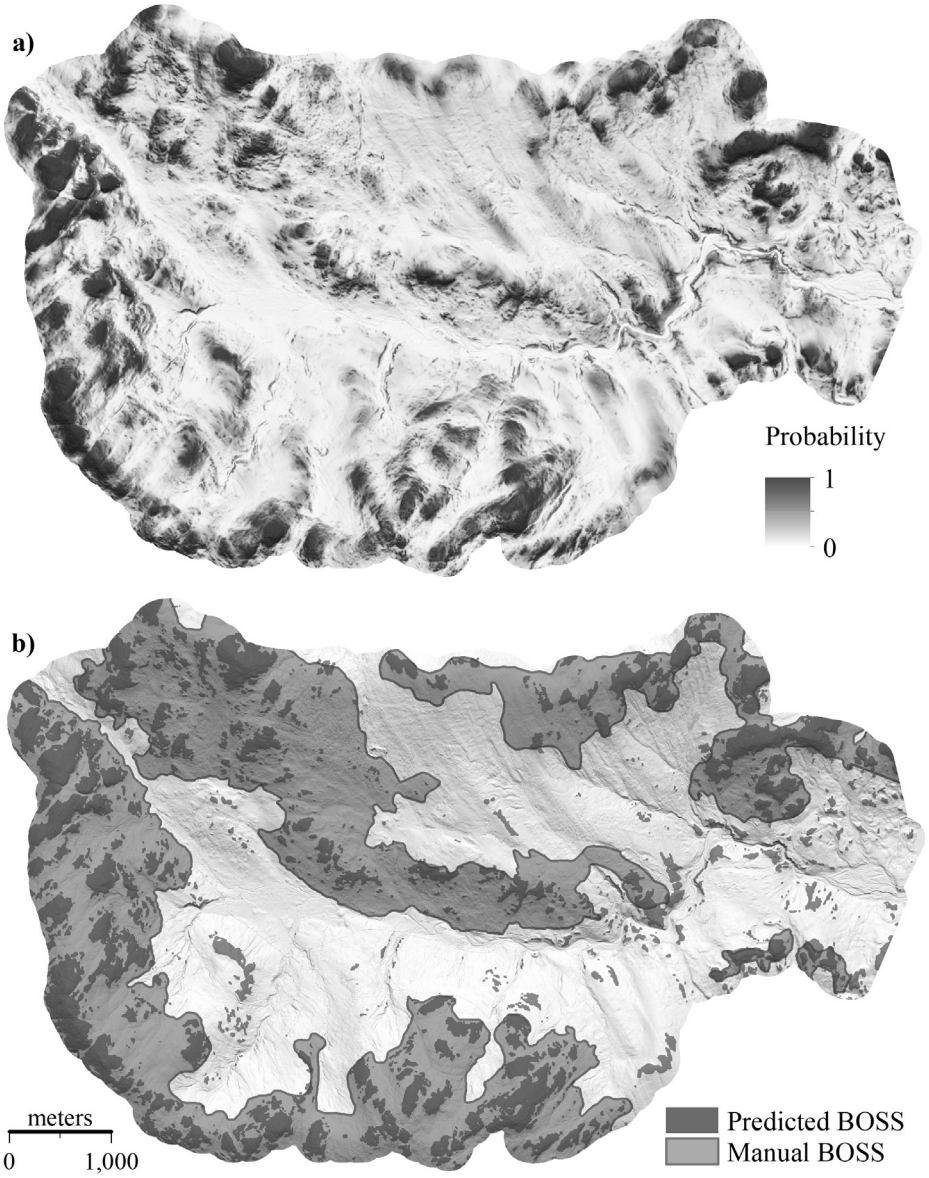

Fig. 4. (a) HBEF catchment depicting probability of BOSS from 0 to 1 with highest probability depicted in dark grey. (b) Predicted BOSS locations depicted in dark grey on a shaded relief (315°) map with manual delineation of BOSS are depicted by lighter grey polygons. Overall agreement on bedrock occurrence is high, however, predicted BOSS suggest higher presence of small pockets in the valley bottom and more scattered pockets of deep soil along the ridges.

performed well predicting rock exposures on rapidly eroding hillslopes in California and Idaho, USA. Scarpone et al. (2017) increased accuracy from 48% of bedrock exposures in manually delineated legacy land cover maps to 88% with the use of a random forest model using 17 predictor variables predictions in southern British Columbia, Canada. Then an independent dataset, created through photo interpretation and *in situ* ground truthing, was used to validate the random forest exposed bedrock model (Sandvoss et al., 2005). The most significant difference between these studies and our work is that we used visually interpreted points for predictive modeling combined with a second distinct study area for model evaluation. In addition, the previous studies were done in rapidly eroding hillslopes or in climatic regions where vegetation was sparse enough to identify bedrock outcrops from aerial photographs and common image processing techniques of aerial imagery were applicable (Grebby et al., 2011). Finally, the success of our methods can likely be attributed to the use of only terrain derivatives as model predictors in a landscape where the current vegetation does not necessarily reflect the vegetation-soil relationships due to extensive land use history. Our methods will be useful both in study areas with small sample sizes and in humid climates where vegetation obscures visualization of outcrops in aerial imagery and where Lidar data can be used to create detailed bare earth surface models.

4.3. Multi-scale topographic metrics

The multiple radii for computing TPI in this study appear to address the challenges of topographic convexity exhibited by bedrock-controlled areas at multiple spatial scales (Behrens et al., 2010; Cavazzi et al., 2013; Levi, 2017, 2017; Lindsay et al., 2015). It can be difficult to determine the radius of generating predictor variables at one specific scale in advance; therefore, multiple window radii have the potential to produce results that do not limit the scope of TPI as a predictor. Although the four classifiers in this study yielded very similar results, GAM had a slightly higher coefficient of agreement and slightly better overall binary probabilistic performance (Fig. 3). Additive models accommodate a range of linear and smooth nonlinear effects of continuous covariates and the model process selects the most suitable covariate. In the case of BOSS, GAM results presented here highlight the

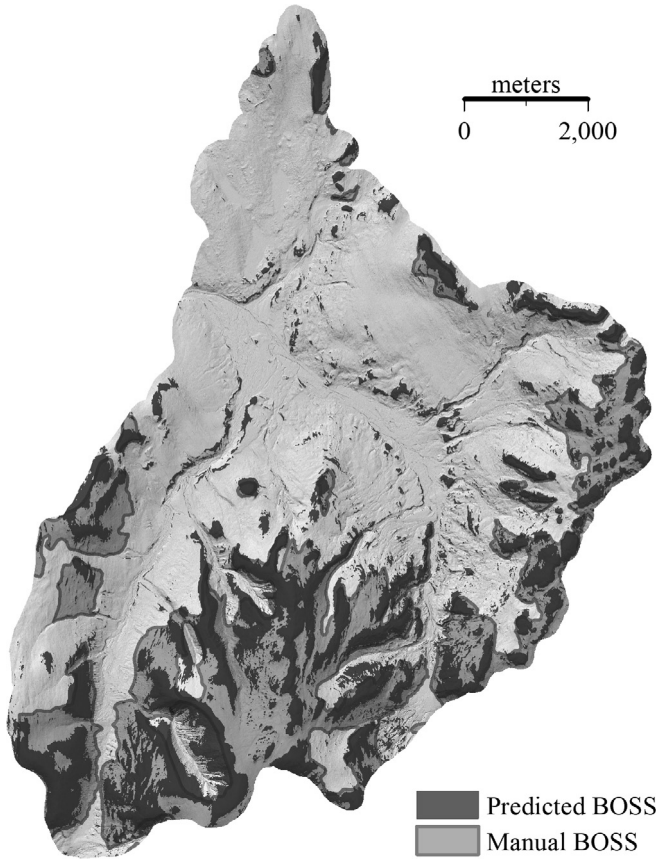

Fig. 5. WAMMO catchment buffered by 200 m depicting GAM predicted bedrock outcrop-shallow soil locations in dark grey. NRCS manual delineation of bedrock-controlled areas is depicted by lighter grey polygons.

nonlinear nature of bedrock outcrops. The combination of these multi-scale covariates increases the complexity of the model, and potentially increases the accuracy, to predict bedrock structure in the landscape (Behrens et al., 2010). It is not surprising that in landscapes with a high degree of topographic complexity, such as the northeastern USA, more than one neighborhood extent would be successful at characterizing pedological processes at multiple scales.

5. Conclusions

Identifying the areal extent of BOSS plays a key role in understanding ecology, hydrology, and soil development. Extracting bedrock outcrop features, however, is especially challenging in landscapes where outcrops are scattered, vegetation is dense, and where associated thin soils constitute a thin mantle over shallow bedrock. Manual methods of delineating BOSS soils are still commonly employed and are expensive to employ over broad areas, limited by geometry of polygon units, and most commonly applied with aerial visualization methods in regions with sparse vegetation cover. The success of this study in leveraging visual interpretation of high-resolution relief maps and automated delineations could be applied to most landscapes with high resolution bare earth surface models. Visual interpretation of hillshade maps resulted in a 79% accuracy of interpreting deep soils and 84% accuracy in distinguishing BOSS. The four classifiers explored in this study yielded very similar results, however, a generalized additive model had a slightly higher overall accuracy, 85%, predicting the presence of BOSS in HBEF and 86% overall accuracy in WAMMO. Manual delineation of polygons of HBEF had 65% overall accuracy and 85% overall accuracy in WAMMO. We were able to significantly improve the efficiency of delineating BOSS presence as well as provide a comparable alternative. This study demonstrates a framework in which to generate a robust sample size from visual interpretation of point locations and model multi-scale processes occurring within upland landscapes. These methods are likely transferable across younger landscapes across the globe where bedrock outcrops create roughness contrasts with adjacent deeper soils.

Declaration of Competing Interest

The authors declare that they have no known competing financial interests or personal relationships that could have appeared to influence the work reported in this paper.

Acknowledgements

We thank Roger DeKett, Jessica Philippe, and Martha Stuart, Natural Resources Conservation Service, for sharing the manually delineated polygons and completing the pedon descriptions on the Wild Ammonoosuc catchment. We also thank all the observers who contributed to the Hubbard Brook soil database. We also acknowledge Robert Colter and co-workers, White Mountain National Forest, for sharing data on the Wild Ammonoosuc catchment. Hubbard Brook Experimental Forest is managed by the USDA Forest Service, Northern Research Station, Newtown Square, PA.

Appendix A. Supplementary data

Supplementary data to this article can be found online at https://doi.org/10.1016/j.geoderma.2020.114495.

References

Asano, Y., Uchida, T., Mimasu, Y., Ohte, N., 2009. Spatial patterns of stream solute concentrations in a steep mountainous catchment with a homogeneous landscape. Water Resour. Res. 45. https://doi.org/10.1029/2008WR007466.

Bailey, A.S., Hornbeck, J.W., Campbell, J.L., Eagar, C., 2003. Hydrometeorological database for Hubbard Brook Experimental Forest: 1955-2000. US Dep. Agric. For. Serv. Northeast. Res. Stn. 305, 36. https://doi.org/10.2737/NE-GTR-305.

Bailey, S.W., Brousseau, P.A., McGuire, K.J., Ross, D.S., 2014. Influence of landscape position and transient water table on soil development and carbon distribution in a steep, headwater catchment. Geoderma 226, 279–289.

Bailey, S.W., McGuire, K.J., Ross, D.S., Green, M.B., Fraser, O.L., 2019. Mineral weathering and podzolization control acid neutralization and streamwater chemistry gradients in upland glaciated catchments, Northeastern United States. Front. Earth Sci. 7. https://doi.org/10.3389/feart.2019.00063.

Bailey, S.W., 2019. Hubbard brook experimental forest: pedon locations, 1995-Present. Environ. Data Initiat. https://doi.org/10.6073/pasta/a7bffc2c0be8052e83b2145993ffa46c.

Beaudette, D.E., Roudier, P., O'Geen, A.T., 2013. Algorithms for quantitative pedology: a toolkit for soil scientists. Comput. Geosci. 52, 258–268. https://doi.org/10.1016/j.cageo.2012.10.020.

Behrens, T., Zhu, A.-X., Schmidt, K., Scholten, T., 2010. Multi-scale digital terrain analysis and feature selection for digital soil mapping. Geoderma 155, 175–185. https://doi.org/10.1016/j.geoderma.2009.07.010.

Belt, K., Paxton, S.T., 2005. GIS as an aid to visualizing and mapping geology and rock properties in regions of subtle topography. GSA Bull. 117, 149–160. https://doi.org/10.1130/B25463.1.

Beven, K.J., Kirkby, M.J., 1979. A physically based, variable contributing area model of basin hydrology/Un modèle à base physique de zone d'appel variable de l'hydrologie du bassin versant. Hydrol. Sci. Bull. 24, 43–69. https://doi.org/10.1080/02626667909491834.

Bourgault, R.R., Ross, D.S., Bailey, S.W., Bullen, T.D., McGuire, K.J., Gannon, J.P., 2017. Redistribution of soil metals and organic carbon via lateral flowpaths at the catchment scale in a glaciated upland setting. Geoderma 307, 238–252. https://doi.org/10.1016/j.geoderma.2017.05.039.

Breiman, L., 2001. Random forests. Mach. Learn. 45, 5–32. https://doi.org/10.1023/A:1010933404324.

Brenning, A., 2008. Statistical geocomputing combining R and SAGA: the example of landslide susceptibility analysis with generalized additive models. Hambg. Beitr. Zur Phys. Geogr. Landschaftsökologie 19, 410.

Brungard, C.W., Boettinger, J.L., Duniway, M.C., Wills, S.A., Edwards, T.C., 2015. Machine learning for predicting soil classes in three semi-arid landscapes. Geoderma 239–240, 68–83. https://doi.org/10.1016/j.geoderma.2014.09.019.

Brus, D.J., Kempen, B., Heuvelink, G.B.M., 2011. Sampling for validation of digital soil maps. Eur. J. Soil Sci. 62, 394–407. https://doi.org/10.1111/j.1365-2389.2011.

01364.x.
Burton, W.C., Walsh, G.J., Armstrong, Thomas R., 2000. Bedrock geologic map of the Hubbard Brook Experimental Forest, Grafton County, New Hampshire: U.S. (Open-File Report No. 00–45). U.S. Geological Survey, Reston, Virginia.
Cavazzi, S., Corstanje, R., Mayr, T., Hannam, J., Fealy, R., 2013. Are fine resolution digital elevation models always the best choice in digital soil mapping? Geoderma 195–196, 111–121. https://doi.org/10.1016/j.geoderma.2012.11.020.
Cohen, J., 1960. A coefficient of agreement for nominal scales. Educ. Psychol. Meas. 20, 37–46. https://doi.org/10.1177/001316446002000104.
Colter, R.A., 2019. Ecological Classification across the White Mountain National Forest using LiDAR (Dissertation). University of New Hampshire, Durham, NH.
Congalton, R.G., 1991. A review of assessing the accuracy of classifications of remotely sensed data. Remote Sens. Environ. 37, 35–46. https://doi.org/10.1016/0034-4257(91)90048-B.
Congalton, R.G., Plourde, L., 2002. Quality assurance and accuracy assessment of information derived from remotely sensed data. In: Manual of Geospatial Science and Technology. Taylor & Francis, London, pp. 349–361.
Conrad, O., Bechtel, B., Bock, M., Dietrich, H., Fischer, E., Gerlitz, L., Wehberg, J., Wichmann, V., Böhner, J., 2015. System for automated geoscientific analyses (SAGA) v. 2.1.4. Geosci. Model Dev. 8, 1991–2007. https://doi.org/10.5194/gmd-8-1991-2015.
DiBiase, R.A., Heimsath, A.M., Whipple, K.X., 2012. Hillslope response to tectonic forcing in threshold landscapes. Earth Surf. Process. Landf. 37, 855–865. https://doi.org/10.1002/esp.3205.
Drăguţ, L., Eisank, C., 2011. Object representations at multiple scales from digital elevation models. Geomorphology 129, 183–189. https://doi.org/10.1016/j.geomorph.2011.03.003.
Fraser, O.L., McGuire, K.J., Bailey, S.W., 2019a. Hubbard Brook Experimental Forest: 5 meter LiDAR-derived Topographic Metrics, 2018. Environ. Data Initiat. Available at: https://portal.edirepository.org/nis/mapbrowse?scope=knb-lter-hbr & identifier=212.
Fraser, O.L., McGuire, K.J., Bailey, S.W., 2019b. Hubbard Brook Experimental Forest: 1 meter LiDAR-derived and Hydro-enforced Digital Elevation Models, 2012. Environ Data Initiat Available at: https://portal.edirepository.org/nis/mapbrowse?packageid=knb-lter-hbr.211.1.
Gannon, J.P., Bailey, S.W., McGuire, K.J., 2014. Organizing groundwater regimes and response thresholds by soils: a framework for understanding runoff generation in a headwater catchment. Water Resour. Res. 50, 8403–8419. https://doi.org/10.1002/2014WR015498.
Gillin, C.P., Bailey, S.W., McGuire, K.J., Gannon, J.P., 2015. Mapping of hydropedologic spatial patterns in a steep headwater catchment. Soil Sci. Soc. Am. J. 79, 440–453. https://doi.org/10.2136/sssaj2014.05.0189.
Grebby, S., Naden, J., Cunningham, D., Tansey, K., 2011. Integrating airborne multispectral imagery and airborne LiDAR data for enhanced lithological mapping in vegetated terrain. Remote Sens. Environ. 115, 214–226. https://doi.org/10.1016/j.rse.2010.08.019.
Guisan, A., Weiss, S.B., Weiss, A.D., 1999. GLM versus CCA spatial modeling of plant species distribution. Plant Ecol. 143, 107–122. https://doi.org/10.1023/A:1009841519580.
Hahm, W.J., Riebe, C.S., Lukens, C.E., Araki, S., 2014. Bedrock composition regulates mountain ecosystems and landscape evolution. Proc. Natl. Acad. Sci. 111, 3338–3343. https://doi.org/10.1073/pnas.1315667111.
Hastie, T.J., Tibrhirani, R.J., Friedman, J., 2009. The Elements of Statistical Learning: DataMining, Inference, and Prediction, second ed. Springer, New York, NY.
Hastie, T.J., Tibshirani, R.J., 1990. Generalized Additive Models, in: Monographs on Statistics and Applied Probability. Chapman and Hall, Hall.
Haugerud, R.A., Harding, D.J., Johnson, S.Y., Harless, J.L., Weaver, C.S., Sherrod, B.L., 2003. High-resolution lidar topography of the Puget Lowland, Washington — a Bonanza for Earth Science. GSA Today 13, 4. https://doi.org/10.1130/1052-5173(2003)13<0004:HLTOTP>2.0.CO;2.
Hengl, T., Rossiter, D.G., Stein, A., 2003. Soil sampling strategies for spatial prediction by correlation with auxiliary maps. Soil Res. 41, 1403–1422. https://doi.org/10.1071/sr03005.
Heung, B., Ho, H.C., Zhang, J., Knudby, A., Bulmer, C.E., Schmidt, M.G., 2016. An overview and comparison of machine-learning techniques for classification purposes in digital soil mapping. Geoderma 265, 62–77. https://doi.org/10.1016/j.geoderma.2015.11.014.
Hjerdt, K.N., McDonnell, J.J., Seibert, J., Rodhe, A., 2004. A new topographic index to quantify downslope controls on local drainage. Water Resour. Res. 40, W05602. https://doi.org/10.1029/2004WR003130.
Humphreys, G.S., Wilkinson, M.T., 2007. The soil production function: A brief history and its rediscovery. Geoderma 139, 73–78. https://doi.org/10.1016/j.geoderma.2007.01.004.
Karlsson, C.S.J., Jamali, I.A., Earon, R., Olofsson, B., Mörtberg, U., 2014. Comparison of methods for predicting regolith thickness in previously glaciated terrain, Stockholm, Sweden. Geoderma 226–227, 116–129. https://doi.org/10.1016/j.geoderma.2014.03.003.
Kleinbaum, D., Kupper, L., Nizam, A., Muller, K., 2013. Applied Regression Analysis and other Multivariable Methods, fifth ed. Cengage Learning, Boston, MA.
Kruckeberg, A.R., 2002. Geology and Plant Life: The Effects of Landforms and Rock Types on plants. University of Washington Press.
Kuhn, M., 2008. Building predictive models in R using the caret package. J. Stat. Softw. 28, 1–26.
Leak, W.B., 1982. Habitat mapping and interpretation in New England. Res Pap NE-496 Broomall PA US Dep. Agric. For. Serv. Northeast. For. Exp. Stn. 28p, 496.
Levi, M.R., 2017. Neighborhood size of training data influences soil map disaggregation. Soil Sci. Soc. Am. J. 81, 354–368. https://doi.org/10.2136/sssaj2016.08.0258.
Lindsay, J.B., Cockburn, J.M.H., Russell, H.A.J., 2015. An integral image approach to performing multi-scale topographic position analysis. Geomorphology 245, 51–61. https://doi.org/10.1016/j.geomorph.2015.05.025.
MacMillan, R.A., Pettapiece, W.W., Nolan, S.C., Goddard, T.W., 2000. A generic procedure for automatically segmenting landforms into landform elements using DEMs, heuristic rules and fuzzy logic. Fuzzy Sets Syst. 113, 81–109. https://doi.org/10.1016/S0165-0114(99)00014-7.
Malone, B.P., Minasny, B., McBratney, A.B., 2017. Using R for digital soil mapping, progress in soil science. In: Malone, B.P., Minasny, B., McBratney, A.B. (Eds.), Continuous Soil Attribute Modeling and Mapping. Springer International Publishing, Cham, pp. 117–149. https://doi.org/10.1007/978-3-319-44327-0_5.
McBratney, A.B., Mendonça Santos, M.L., Minasny, B., 2003. On digital soil mapping. Geoderma 117, 3–52. https://doi.org/10.1016/S0016-7061(03)00223-4.
McNamara, J.P., Tetzlaff, D., Bishop, K., Soulsby, C., Seyfried, M., Peters, N.E., Aulenbach, B.T., Hooper, R., 2011. Storage as a metric of catchment comparison. Hydrol. Process. 25, 3364–3371. https://doi.org/10.1002/hyp.8113.
Meyer, M.D., North, M.P., Gray, A.N., Zald, H.S.J., 2007. Influence of soil thickness on stand characteristics in a Sierra Nevada mixed-conifer forest. Plant Soil 294, 113–123. https://doi.org/10.1007/s11104-007-9235-3.
Milodowski, D.T., Mudd, S.M., Mitchard, E.T.A., 2015. Topographic roughness as a signature of the emergence of bedrock in eroding landscapes. Earth Surf. Dyn. 3, 483–499. https://doi.org/10.5194/esurf-3-483-2015.
Minasny, B., McBratney, Alex, B., 2016. Digital soil mapping: A brief history and some lessons. Geoderma, Soil mapping, classification, and modelling: history and future directions 264, 301–311. https://doi.org/10.1016/j.geoderma.2015.07.017.
Nauman, T.W., Thompson, J.A., Teets, S.J., Dilliplane, T.A., Bell, J.W., Connolly, S.J., Liebermann, H.J., Yoast, K.M., 2015. Ghosts of the forest: Mapping pedomemory to guide forest restoration. Geoderma 247–248, 51–64. https://doi.org/10.1016/j.geoderma.2015.02.002.
R Development Core Team, 2018. R: A language and environment for statistical computing. R Found. Stat. Comput. Version 3.5.1.
Riley, S.J., 1999. Index that quantifies topographic heterogeneity. Intermt. J. Sci. 5, 23–27.
Sandvoss, M., McClymond, B., Farnden, C., 2005. User's Guide to the Vegetation Resources Inventory (technical report). Government of British Columbia.
Sappington, J.M., Longshore, K.M., Thompson, D.B., 2007. Quantifying landscape ruggedness for animal habitat analysis: a case study using bighorn sheep in the Mojave Desert. J. Wildl. Manag. 71, 1419–1426. https://doi.org/10.2193/2005-723.
Scarpone, C., Schmidt, M.G., Bulmer, C.E., Knudby, A., 2017. Semi-automated classification of exposed bedrock cover in British Columbia's Southern Mountains using a Random Forest approach. Geomorphology 285, 214–224. https://doi.org/10.1016/j.geomorph.2017.02.013.
Schoeneberger, P.J., 2012. Field book for describing and sampling soils. Natural Resources Conservation Service, National Soil Survey Center, Lincoln, NE.
Schwarz, P.A., Fahey, T.J., Martin, C.W., Siccama, T.G., Bailey, A., 2001. Structure and composition of three northern hardwood–conifer forests with differing disturbance histories. For. Ecol. Manag. 144, 201–212. https://doi.org/10.1016/S0378-1127(00)00371-6.
Seibert, J., McGlynn, B.L., 2007. A new triangular multiple flow direction algorithm for computing upslope areas from gridded digital elevation models. Water Resour. Res. 43. https://doi.org/10.1029/2006WR005128.
Shangguan, W., Hengl, T., Mendes de Jesus, J., Yuan, H., Dai, Y., 2017. Mapping the global depth to bedrock for land surface modeling: Global Map of Depth to Bedrock. J. Adv. Model. Earth Syst. 9, 65–88. https://doi.org/10.1002/2016MS000686.
Sheffer, E., von Hardenberg, J., Yizhaq, H., Shachak, M., Meron, E., 2013. Emerged or imposed: a theory on the role of physical templates and self-organisation for vegetation patchiness. Ecol. Lett. 16, 127–139. https://doi.org/10.1111/ele.12027.
Shi, X., Long, R., Dekett, R., Philippe, J., 2009. Integrating different types of knowledge for digital soil mapping. Soil Sci. Soc. Am. J. 73, 1682–1692. https://doi.org/10.2136/sssaj2007.0158.
Siccama, T.G., Fahey, T.J., Johnson, C.E., Sherry, T.W., Denny, E.G., Girdler, E.B., Likens, G.E., Schwarz, P.A., 2007. Population and biomass dynamics of trees in a northern hardwood forest at Hubbard Brook. Can. J. For. Res. 37, 737–749. https://doi.org/10.1139/X06-261.
Smith, M.-L., 1995. Community and edaphic analysis of upland northern hardwood communities, central Vermont. USA. For. Ecol. Manag. 72, 235–249. https://doi.org/10.1016/0378-1127(94)03456-7.
Soil Science Division Staff, 2017. Soil survey manual, C. Ditzler, K. Scheffe, H.C. Monger (Eds.). ed. USDA Handbook, 18, Government Printing Office, Washington, DC.
Sommer, M., Halm, D., Geisinger, C., Andruschkewitsch, I., Zarei, M., Stahr, K., 2001. Lateral podzolization in a sandstone catchment. Geoderma 103, 231–247. https://doi.org/10.1016/S0016-7061(01)00018-0.
Sommer, M., Halm, D., Weller, U., Zarei, M., Stahr, K., 2000. Lateral Podzolization in a Granite. Landscape 64, 1434–1442. https://doi.org/10.2136/sssaj2000.6441434x.
Stage, A.R., 1976. An expression for the effect of aspect, slope, and habitat type on tree growth. For. Sci. 22, 457–460. https://doi.org/10.1093/forestscience/22.4.457.
Tesfa, T.K., Tarboton, D.G., Chandler, D.G., McNamara, J.P., 2009. Modeling soil depth from topographic and land cover attributes. Water Resour. Res. 45. https://doi.org/10.1029/2008WR007474.
Travis, M.R., Elsner, G.H., Iverson, W.D., Johnson, C.G., 1975. VIEWIT: computation of seen areas, slope, and aspect for land-use planning. Gen Tech Rep PSW-GTR-11 Berkeley CA Pac. Southwest Res. Stn. For. Serv. US Dep. Agric. 70 P 011.
Webster, T.L., Murphy, J.B., Gosse, J.C., Spooner, I., 2006. The application of lidar-derived digital elevation model analysis to geological mapping: an example from the Fundy Basin, Nova Scotia. Canada. Can. J. Remote Sens. 32, 173–193. https://doi.

org/10.5589/m06-017.
Wood, S.N., 2004. Stable and efficient multiple smoothing parameter estimation for generalized additive models. J. Am. Stat. Assoc. 99, 673–686. https://doi.org/10.1198/016214504000000980.
Zevenbergen, L.W., Thorne, C.R., 1987. Quantitative analysis of land surface topography. Earth Surf. Process. Landf. 12, 47–56.
Zhu, A.X., Hudson, B., Burt, J., Lubich, K., Simonson, D., 2001. Soil mapping using GIS, expert knowledge, and fuzzy logic. Soil Sci. Soc. Am. J. 65, 1463. https://doi.org/10.2136/sssaj2001.6551463x.